**ORIGINAL ARTICLE**

# Morphological changes and altered expression of antioxidant proteins in a heterozygous dynein mutant; a mouse model of spinal muscular atrophy

**Larisa M. Wiggins**

*Department of Physiology and Cell Biology, University of Nevada, Reno,* ***United States***

**Received** June 26, 2014
**Accepted** July 31, 2014

**Published Online** October 17, 2014

**DOI** 10.5455/oams.310714.or.071

**Corresponding Author**
Larisa M. Wiggins
University of Nevada School of Medicine, 1664 North Virginia Street, MS 352, Reno, NV 89557, USA.
lwiggins@medicine.nevada.edu

**Key Words**
Neurodegeneration; Neuroinflammation; Peroxiredoxin; Spinal muscular atrophy; SMA-LED

**Abstract**

***Objective:*** There is increased evidence that oxidative stress is involved in exacerbations of neurodegenerative diseases and spinal muscular atrophies.

***Methods:*** We examined changes in morphology and expression of antioxidant proteins and peroxiredoxins in motor neurons of lumbar spinal cord, dorsal root ganglion sensory neurons, macroglial cells and quadriceps muscles of newborn heterozygous Loa/+ mice ("legs at odd angles"), a mouse model for early onset of the spinal muscular atrophy with lower extremity predominance (SMA-LED).

***Results:*** Our data indicate that newborn Loa-mice develop: neuroinflammation of the sensory and motor neurons; muscular inflammation with atrophic and denervated myofibers; increased expression of neuronal mitochondrial peroxiredoxins (Prxs) 3, 5 and cytoplasmic Prx 6 in motor and sensory neurons, myofibers, fibroblasts of perimysium and chondrocytes of cartilage; and decreased expression of Prx 6 by glial cells and in extracellular space surrounding motor neurons.

***Conclusion:*** The decrease in expression of Prx 6 by glial cells and extracellular Prx 6 secretion in early stages of the pathological conditions is consistent with the hypothesis that chronic oxidative stress may lead to neurodegeneration of motor neurons and exacerbation of the pathology.



## INTRODUCTION

### Spinal muscular atrophy-lower extremity, dominant (SMA-LED)

Mutations in the tail domain of the heavy chain of cytoplasmic dynein *DYNC1H1* gene are the cause of spinal muscular atrophy with lower extremity predominance (SMA-LED) [1]. SMA-LED is a rare, degenerative, inherited disease [1, 2]. Typical clinical features in patients with the SMA-LED include: late infantile motor development, unstable gait, proximal lower limb-dominant muscle weakness or atrophy and difficulty squatting [1, 3, 4].

Muscle computer tomography demonstrated severe atrophy and lipid degeneration, predominantly in the bilateral quadriceps femoris [3]. A muscle biopsy demonstrated chronic denervation, accumulation of inflammatory cells surrounding perimysial blood vessels, a massive increase in the amount of fibrous tissue and enlarged type 1 fibers [3, 4]. Additionally, a magnetic resonance imaging of the thigh muscles demonstrated diffuse atrophy and fat replacement in young patients [5]. All these findings indicate that hallmarks of the SMA-LED are early childhood onset of degeneration of spinal cord motor neurons, proximal leg weakness with muscle atrophy and non-length-dependent motor neuron disease without sensory involvement [1, 3, 4].

### Loa/+ mice and evidence of oxidative stress

The Loa/+ mouse ("legs at odd angles") is a well-established model of SMA-LED. These mice have a dynein mutation of the *DYNC1H1* gene and show disruption in transport of neuronal cargoes. Loa/+ mice may represent an ideal system to model the pathophysiological effects of the SMA-LED human mutation [6]. The heterozygous Loa/+ mice develop pathological features similar to the SMA-LED early onset: abnormal motor neuron innervation, decreased number of spinal cord ventral horn motor neurons, motor neuron degeneration, impaired coordination, abnormal grip strength, muscle spasms, accumulation of fat in tissues and abnormal mitochondrial morphology and function [7-10]. Typical pathological findings in heterozygous Loa/+ mice include early-onset degeneration of spinal motor neurons and proprioceptive sensory neuropathy, muscle spindle deficiency, neuromuscular junction defects, neuronal migration, alteration of axonal transport of cargoes, abnormalities due to alteration of the morphology of motor neurons and vacuolar mitochondria [8, 11-13]. It was proposed that such changes in morphology of mitochondria correlate with oxidative stress in other neurodegenerative diseases with imbalance between oxidant and antioxidant proteins [14-16].

Mitochondrial dysfunction and oxidative stress are one of the main mechanisms associated with the pathogenesis of other neurodegenerative diseases, pathological conditions and aging [15, 17-20]. Recent studies show that Prxs 3 and 5 are major mitochondrial antioxidant proteins in the brain [21-23]. Prx 6 is an antioxidant protein widely expressed in all tissues, with unique ability to inactivate reactive oxygen species (ROS) and lipid peroxides [24, 25]. Under physiological conditions astrocytes express and secrete Prx 6 in the extracellular space in the anterior horn of the spinal cord [26] or brain [27] to protect neuronal DNA, proteins and lipids from oxidative damage and prevent neuronal loss and both astrocytes and oligodendrocytes in adult mouse brain [28]. Altered expression of Prx 6 in the central nervous system (CNS) was shown in neurodegenerative [29] and neurological diseases [30], experimental cerebral ischemic damage [31] and experimental spinal cord damage [32]. Moreover, increased oxidative stress was described in white adipose tissue of Loa/+ mice [10].

Because of increasing evidence that oxidative stress can be involved in pathology of SMA-LED, we conducted an analysis of the expression of antioxidant proteins, Prxs 3, 5 and 6, in lumbar spinal neurons and quadriceps muscle of newborn Loa/+ mice and determined whether morphological and ultrastructural changes occur.

## MATERIAL AND METHODS

### Mice

Data were derived from six heterozygous newborn Loa/+ pups and two newborn wild type littermates (congenic on a C57BL/6J background). The animal breeding and studies reported in this paper were carried out under license from the UK Home Office (Animals Scientific Procedures Act 1986) and local ethical review panel under the guidance issued by the Medical Research Council and for the tissue processing and analysis at the University of Nevada, Reno, from UNR's institutional animal care and use committee.

### Genotyping

Forward (TGCTGTGTGCTCTCCTGTTT) and reverse (TTTTACAAGCTTGGCTTTGC) primers were used to amplify a 696 bp product encompassing the Loa mutation site. The polymerase chain reaction (PCR) conditions were 35 cycles at 95°C for 30 sec, 62°C for 30 sec and 72°C for 1 min. The Loa mutation introduces an additional RSA1 restriction site within the 696 bp product and thus PCR products were digested with RSA1 (New England Biolabs) for 2 h at 37°C. Products were run on a 2% agarose gel to determine the genotypes.

### Histology

Newborn mice were anesthetized and fixed with 4% paraformaldehyde for storage. Fixed mice were dissected (quadriceps muscles from both legs and whole segment of lumbar spinal cord from all eight mice), dehydrated in graded ethanols, cleared in xylene, and embedded in paraffin (Paraplast Plus). Paraffin blocks were cut and 5 µm thick sections were collected on silane-coated slides (Surgipath Snowcoat X-tra) and immunostained and counterstained with 0.01% thionin to perform morphological and quantitative immunohistochemical analysis.

### Morphometric analysis

For quantification of connective tissue in muscles, we randomly sampled five counting boxes from ten sections per muscle. We measure the fractional area of connective tissue by using point counting the size of one counting box = 0.16 $mm^2$ per box was 100%. For quantification of number of myofibers with central location of nucleus or atrophic myofibers, we counted the number of these myofibers in one counting box = 0.16 $mm^2$. Five counting boxes per section were randomly selected from ten sections per muscle.

### Immunohistochemistry (IHC)

Mouse spinal cord, thigh muscle and muscular tender tissues were fixed with 4% paraformaldehyde. Five-micrometer paraffin sections were collected, de-paraffinized in xylene and hydrated in ethanol series. Sections were incubated with 3% hydrogen peroxide for 30 min to block endogenous peroxidase activity, and then nonspecific binding sites were blocked with 2.5% normal horse serum in phosphate buffer for 20 min. Sections were washed in phosphate buffer (pH 7.5) and incubated with rabbit primary antibody against Prx 6 (Abcam, ab73350) at a concentration of 1 µg/ml, or rabbit primary antibody against Prx 3 (Abcam, ab73349) at a concentration of 5 µg/ml, or rabbit primary antibody against Prx 5 (Abcam, ab140926) diluted 1/200. Then, sections were incubated for 30 min with ImmPRESS™ reagent (anti-rabbit secondary antibody; Vector Laboratories, UK: #MP-7401). The complex was visualized with ImmPACT™ DAB (peroxidase substrate solution; Vector Laboratories, UK: #SK-4105). Then, sections were counterstained with 0.01% thionin, cleared (ethanol, xylene) and mounted with a neutral plastic resin dissolved in xylene and containing di-n-butyl phthalate as a plasticiser (DBP; in xylene: DPX).

We used negative control to test for the specificity of the antibodies by checking staining after omitting the primary antibody. After IHC reaction, these sections were digitized and analyzed at the light microscopy level with NIS-Elements software (Nikon) for quantification to compare the levels of expression of Prxs 3, 5 and 6 by measuring values of pixel intensity.

 **DOI** 10.5455/oams.310714.or.071

**Quantitative immunohistochemistry (Q-IHC)**

A Q-IHC analysis was employed to determine levels of expression of Prxs in the neurons of lumbar spinal cord, thigh muscle and muscular tender tissues. RGB images acquired by NIS-Elements software were analyzed before saving and converting to JPG format.

After IHC, sections contain different levels of chromogen, from light brown to brown in wild type (WT) mice sections, and from light brown to almost black in Loa/+ mice. The chromogen quantity was determined by reciprocal pixel intensity in percentage where "white area" (area without tissue) have maximal pixel intensity (100%). The detailed protocol for calculation of the reciprocal pixel intensity is available online [33].

To avoid bias, we used manual "point analysis" of selected cells in each image. This is different from the Q-IHC method which measured "area analysis" by normalizing energy of the area per pixel [34]. We measured pixel intensity in three areas: ***(1)*** area of interest; ***(2)*** "white area", area without tissue for each slide; ***(3)*** negative control sections for each sample. To minimize background we used counterstaining with thionin, which stained tissue with light blue color. Previously, not significant differences were detected in chromogen quantity with and without counterstaining [34].

To calculate the chromogen quantity, we subtracted the combine pixel intensity (%) of area of interest of experimental image and homologous region of negative control from pixel intensity (%) of "white area" of each section. Pixel intensity from twenty cells was collected from each section. Data from a minimum of 200 cells (such as neurons, glial cells, fibroblast, myofibers and chondrocytes) was compared for each condition (WT and Loa/+ mice). To prevent observer bias, sections were coded to ensure that the observer was blind to their condition. To determine P values for statistical significance an unpaired two-tailed Student's t-test was used, and P values were calculated using SigmaStat software (Jandel Scientific). The significance level was set at $P < 0.05$.

**Electron microscopy**

Newborn mice were anesthetized and fixed with 4% paraformaldehyde for storage. Fixed mice, in 2% paraformaldehyde and 3% glutaraldehyde (GA) in 0.1 M sodium cacodylate buffer (pH 7.3) were dissected (quadriceps muscles and lumbar spinal cord), postfixed in 1% osmium tetroxide, dehydrated in graded ethanols, treated with propylene oxide and embedded in Spurr resin. Resin blocks were cut and 1 μm thick sections were collected on glass slides and stained with 1% toluidine blue for morphological analysis by using a Nikon light microscope equipped with NIS-Elements software for quantitative analysis and for orientation and selection of areas for further ultrastructural examination. Ultrathin sections (80 nm) were stained with 2.5% aqueous lead citrate and uranyl acetate. Sections were examined and digitized in a Philips CM10 transmission electron microscope equipped with a Gatan 792 BioScan digital imaging system.

We determined the fractional area of cytoplasm with polyribosomes as was described previously [15]. For quantification of the number of damaged mitochondria in cell bodies of motor neurons, we counted the number of these mitochondria in one counting box = 2.25 $\mu m^2$. Twenty counting boxes per one section were randomly selected from ten sections per muscle. The total area of cell bodies of motor neurons sampled in WT and Loa/+ mice with 20 neurons was 450 $\mu m^2$.

## RESULTS

To identify early morphological changes of pathological conditions we compared newborn Loa/+ and WT mice at both light and electron microscopic levels.

**Morphometry at the light-microscopic level**

***Lumbar sensory and motor neurons of the spinal cord***

Alpha motor neurons were identified by their size (more than 13 μm in diameter, [10]) and specific location in the ventral horn (Figs.1ABDEF). Neuroinflammation in newborn Loa/+ mice was determined by two morphological features: ***(1)*** significantly increased size of sensory neurons in Loa/+ mice in comparison to WT mice (12.2 ± 2.8 μm; 5.9 ± 0.5 μm), and ***(2)*** accumulation of activated microglia around motor neurons in Loa/+ mice (Fig.1B). The status of "activated" microglia was determined by ultrastructural features (see below in 'electron microscopy' subsection).

***Quadriceps muscle***

To compare published data of human quadriceps muscle pathology in SMA-LED with data from Loa/+ mice we performed morphological analysis of the same muscle in Loa/+ mice.

Our data indicate early pathological changes in the muscles of newborn Loa/+ mice. The quadriceps muscle displays several pathological features: increased amount of connective tissue between myofibers (5 ± 1% in WT, 16 ± 4% in Loa/+ mice), which is typical for muscular inflammation, fibrosis and dystrophy; increased number of atrophic myofibers (1 ± 0.5% in WT, 4.5 ± 2.5% in Loa/+ mice), which is an early sign of muscle dystrophy; and also increased number of myofibers with central position of the nucleus (2.5 ± 1.3% in WT, 12.1 ± 5% in Loa/+ mice) which is typical for both fibrosis and dystrophy (data are mean ± SEM; Fig.2) [35].

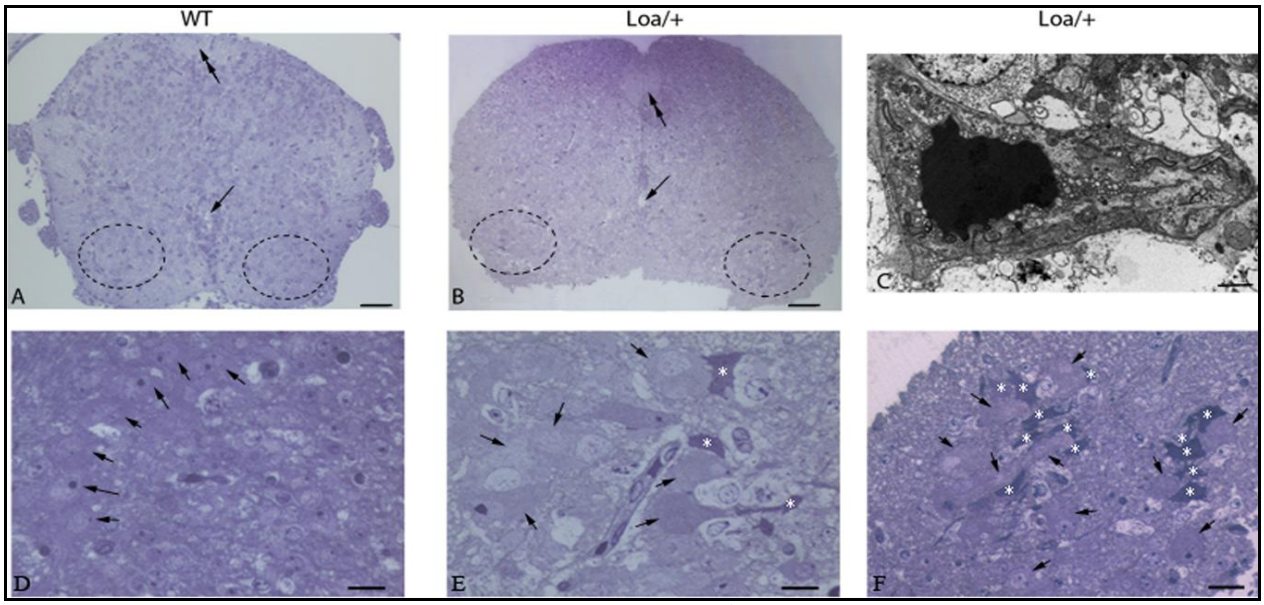


**Figure 1.** Activated microglia in close vicinity to motor neurons in the spinal cord of Loa/+ mice. **(A)** WT mouse, and **(B)** Loa/+ mouse: location of ventral alpha motor neurons; resin sections were stained with toluidine blue; scale bar = 150 µm; posterior median sulcus **(double arrows)**, central canal **(arrows)**, ventral **(anterior)**, and horn **(doted areas)**. **(C)** Ultrastructural features of activated microglia; ultrathin sections were stained with uranyl acetate and lead citrate; scale bar = 1 µm. **(D)** WT mouse; motor neurons **(arrows)** at the light-microscopic level; scale bar =5 µm. **(EF)** Loa/+ mouse; activated microglia **(asterisks)** close to motor neurons **(arrows)** at the light-microscopic level, scale bar = 5-10 µm for E-F, respectively.

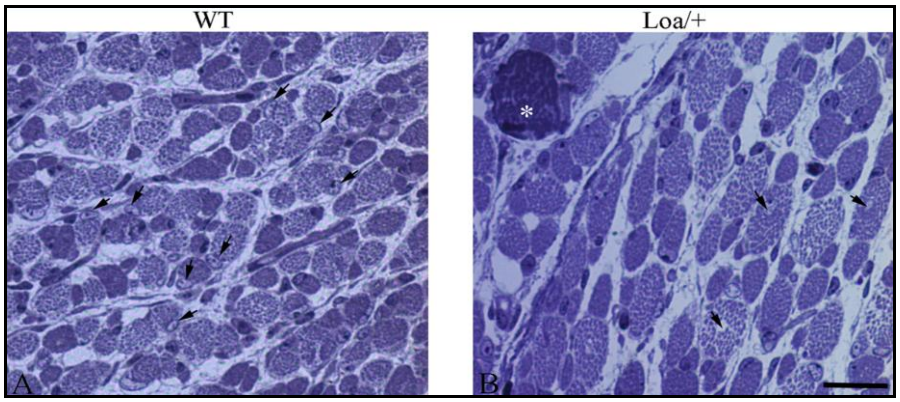


**Figure 2.**
Micrographs illustrate pathological features of thigh muscle of Loa/+ mice. **(A)** WT mouse; note the peripheral position of the nuclei **(arrows)**. **(B)** Loa/+ mouse; note one atrophic myofibers **(asterisks)** and myofibers with central position of the nucleus **(arrow)**.
This panel also shows increase of the connective tissue between myofibers. Scale bar =30 µm.

## Electron microscopy

### *Sensory and motor neurons*

Ultrastructural analysis of sensory and motor neurons showed early alteration in morphology of newborn Loa/+ mice. The pathological changes were similar for both types of neurons, but in the motor neuron they were severe. Ultrastructural images of lumbar sensory and motor neurons show signs of neuroinflammation: increased number of damaged mitochondria (9 ± 2.4% in WT, 20 ± 6.1% in Loa/+ mice); decreased number of polyribosomes (55 ± 5% area of all cytoplasm in WT, 35 ± 2% in Loa/+ mice); elongation of smooth endoplasmic reticulum and a relocation of heterochromatin accumulations from center to neuronal nuclear membranes and appearance of nuclear invaginations and inclusions in Loa/+ neurons (Fig.3).

### *Activated microglia*

Another distinguished feature of spinal motor neurons in Loa/+ mice was the accumulation of microglial cells. Detailed ultrastructural analysis of these microglial cells shows increased numbers of secretory granules and increased size of cell body, which is typical for activated microglial cells during acute neuro-inflammation [36]. Increased number and accumulation of activated microglia (macrophages in CNS) near motor neurons indicate that these neurons are experiencing severe neuroinflammation. Ultrastructure features of activated microglia (Fig.1C) and other alteration at morphology of sensory and motor neurons (Fig.3) are similar to what was described after injection of brain lipopolysaccharide (LPS), a component of outer membrane of Gramm-negative bacteria which induce inflammation and increase oxidative stress [36].

 **DOI** 10.5455/oams.310714.or.071

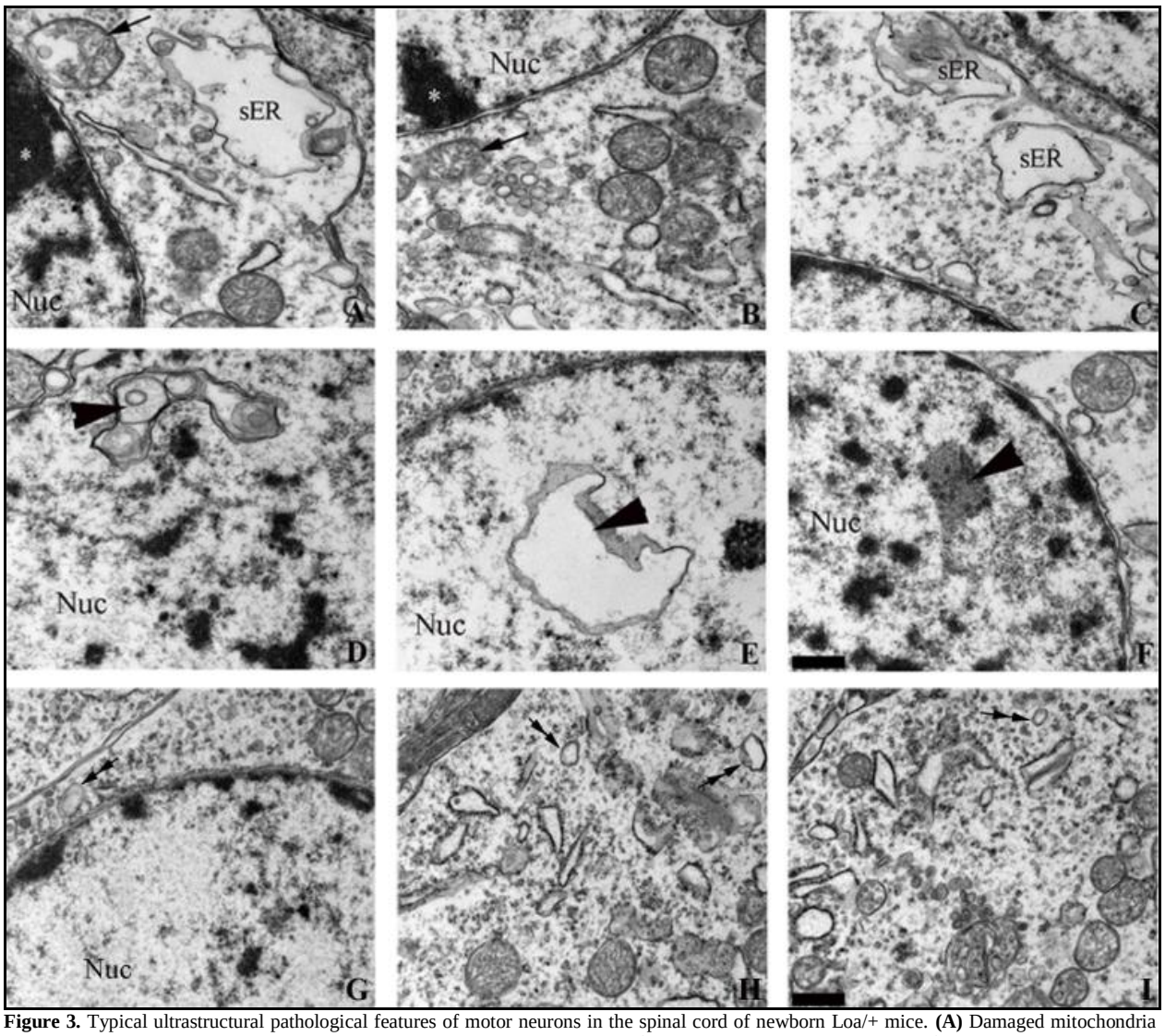


**Figure 3.** Typical ultrastructural pathological features of motor neurons in the spinal cord of newborn Loa/+ mice. **(A)** Damaged mitochondria **(arrow)** and elongated smooth endoplasmic reticulum **(sER)** in the cytoplasm of a motor neuron and accumulation of heterochromatin **(asterisk)** close to the nuclear membrane of the nucleus **(Nuc)**. **(B)** Damaged mmitochondria **(arrow)** in the cytoplasm of a motor neuron and accumulation of heterochromatin **(asterisk)** close to the nuclear membrane of the nucleus **(Nuc)**. **(C)** Elongated smooth (sER) in the cytoplasm of a motor neuron. **(DE)** Nuclear invaginations **(arrowheads)** close to the nuclear membrane of the nucleus **(Nuc)**. **(F)** Nuclear inclusion **(arrowhead)** in the nucleus **(Nuc)**. **(G)** Normal distribution of heterochromatin in the nucleus **(Nuc)** and normal size of smooth endoplasmic reticulum **(double arrows)** in the cytoplasm of newborn WT mice. **(HI)** Normal size of smooth endoplasmic reticulum **(double arrows)** in the cytoplasm of newborn WT mice. (Scale bars = 0.5 mm)

## Quantitative immunohistochemistry

Increased numbers of damaged mitochondria in motor and sensory neurons can be a result of increased oxidative stress due to imbalance in generation of ROS and expression of antioxidant proteins, peroxiredoxins. To compare the levels of expression of mitochondrial antioxidant proteins, Prxs 3 and 5, cytoplasmic Prx 6 and secretory Prx 6, we performed a Q-IHC analysis. The comparison of pixel intensity after IHC identifies several significant changes in expression of these antioxidant proteins in newborn Loa/+ mice.

### *Peroxiredoxin 3*

Expression of mitochondrial Prx 3 in newborn Loa/+ mice showed a statistically significant increase in motor neurons compared to WT mice (45.48 ± 1.09% *vs* 15 ± 1.5%, P = 0.001), in glia around motor neurons (37.71 ± 3.54% *vs* 18.17 ± 1.37%, P = 0.047), in sensory neurons (64.67 ± 0.86% *vs* 43.3 ± 1.48%, P = 0.022; Figs.4GH). Expression of Prx 3 in newborn Loa/+ mice did not show statistically significant changes in glia around sensory neurons (P = 0.343).

### *Peroxiredoxin 5*

Expression of mitochondrial Prx 5 in newborn Loa/+ mice showed a statistically significant increase in motor neurons compared with WT mice (24.3 ± 1.65% *vs* 11.86 ± 0.8%, P = 0.011; Figs.4AB). Expression of

Prx 5 was not significantly different in glia around motor neurons (P = 0.502) or in sensory neurons (P = 0.432). Expression of Prx 5 was not significantly changed in glia around sensory neurons (P = 0.061).

***Peroxiredoxin 6***

*Lumbar spinal cord:* expression of cytoplasmic Prx 6 in newborn Loa/+ mice showed a statistically significant increase in motor neurons compared to WT mice (39.36 ± 2.17% *vs* 23.7 ± 1.78%, P = 0.001; Figs.4CD, Fig.5A) and in glial cells around sensory neurons (41.89 ± 1.73% *vs* 28.57 ± 2.77%, P = 0.02; Figs.4EF, Fig.5F). Expression of cytoplasmic Prx 6 was significantly decreased in glia surrounding motor neurons (37.92 ± 3.62% *vs* 59.63 ± 4.63%, P = 0.001, (Figs.4CD, Fig.5B). Expression of Prx 6 was not significantly different in sensory neurons (P = 0.209, (Fig.5E). The secretory Prx 6 in the extracellular space between motor neurons was decreased in Loa/+ mice (10.51 ± 1.16% *vs* 24.95 ± 2.05%, P = 0.001, Figs.4CD, Fig.5C).

Surprisingly, both macroglial cells astrocytes and oligodendrocytes, surrounding motor neurons expressed Prx 6 in WT mice. We determined the expression of Prx 6 in macroglia in white matter of lumbar spinal cord of WT mice. Our data show that oligodendrocytes expressed more cytoplasmic Prx 6 than astrocytes (83.4 ± 1.03% *vs* 71.67 ± 2.4%). Using morphological criteria at the light microscopic level to identify astrocytes and oligodendrocytes we analyzed expression of Prx 6 separately in macroglial cells to identify which macroglial cells participate in expression of secretory Prx 6 in extracellular space between motor neurons. Both macroglial cells types in Loa/+ mice showed significantly decreased expression of Prx 6; however, there was a dramatic decrease in oligodendrocytes (P = 0.001). Further experiments are required to clarify the role of macroglial cells on reduction of secretory Prx 6 in extracellular space between motor neurons.

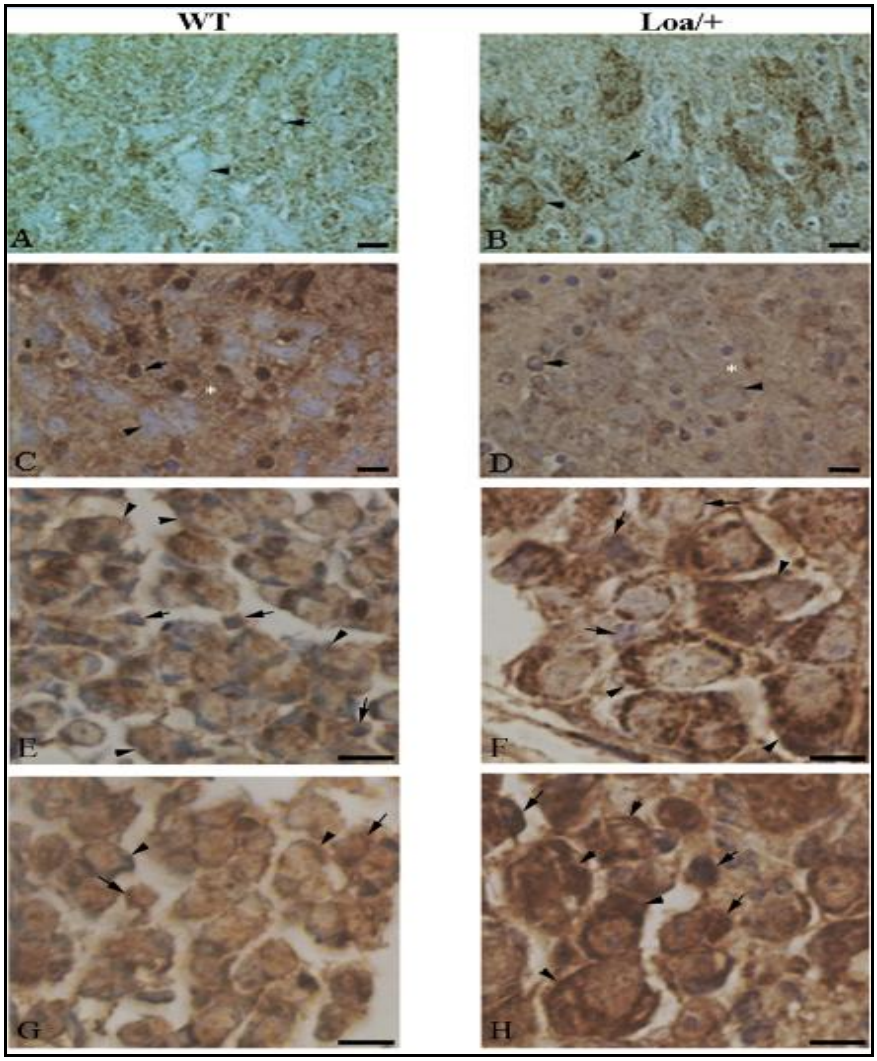


**Figure 4.**
Immunohistochemical analysis of spinal cord motor neurons **(A-D)** and dorsal root ganglion sensory neurons **(E-H)**.
**(A)** Expression of Prx 5 in motor neurons **(arrowhead)** and glial cells **(arrow)** in WT mouse.
**(B)** Increased expression of Prx 5 in motor neurons **(arrowhead)** and glial cells **(arrow)** in Loa/+ mouse.
**(C)** Expression of Prx 6 in motor neurons **(arrowhead)**, glial cells **(arrow)**, and extracellular space surrounding motor neurons **(asterisk)** in WT mouse.
**(D)** Increased expression of Prx 6 in neurons **(arrowhead)**, decreased expression of Prx 6 in glia **(arrow)** and extracellular space surrounding motor neurons **(asterisk)** in Loa/+ mouse.
**(E)** Expression of Prx 6 in sensory neurons **(arrowheads)** and glial cells **(arrows)** in WT mouse.
**(F)** Increased expression of Prx 6 in sensory neurons **(arrowhead)** and glia cells **(arrow)** in Loa/+ mouse; also note increased size of sensory neurons.
**(G)** Expression of Prx 3 in sensory neurons **(arrowheads)** and glia cells **(arrow)** in WT mouse.
**(H)** Increased expression of Prx 3 in sensory neurons **(arrowheads)** and glial cells **(arrow)** in Loa/+ mouse; also note increased size of sensory neurons.
All scale bars 10 mm.

 **DOI** 10.5455/oams.310714.or.071

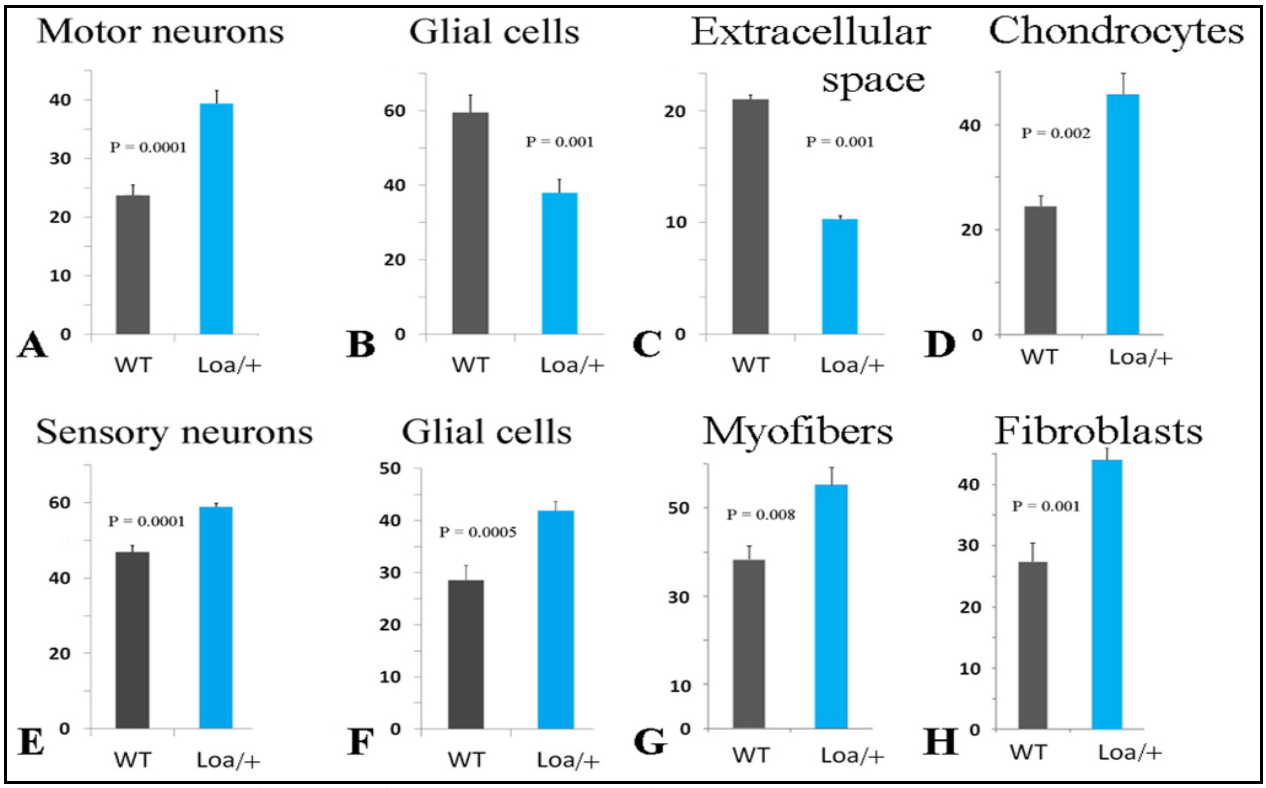


**Figure 5.** Q-IHC analysis of expression of Prx 6. **(A)** Motor neurons of lumbar spinal cord; **(B)** glia cells surrounding motor neurons; **(C)** extracellular space surrounding motor neurons; **(D)** chondrocytes of tendon of quadriceps muscle; **(E)** dorsal root ganglion sensory neurons; **(F)** glia cells surrounding sensory neurons; **(G)** myofibers of quadriceps muscle; and **(H)** fibroblasts of perimysium of quadriceps muscle. (Y-axis indicates pixel density in %; the error bars are SEM; and P values for statistical significance are calculated by Student's test.)

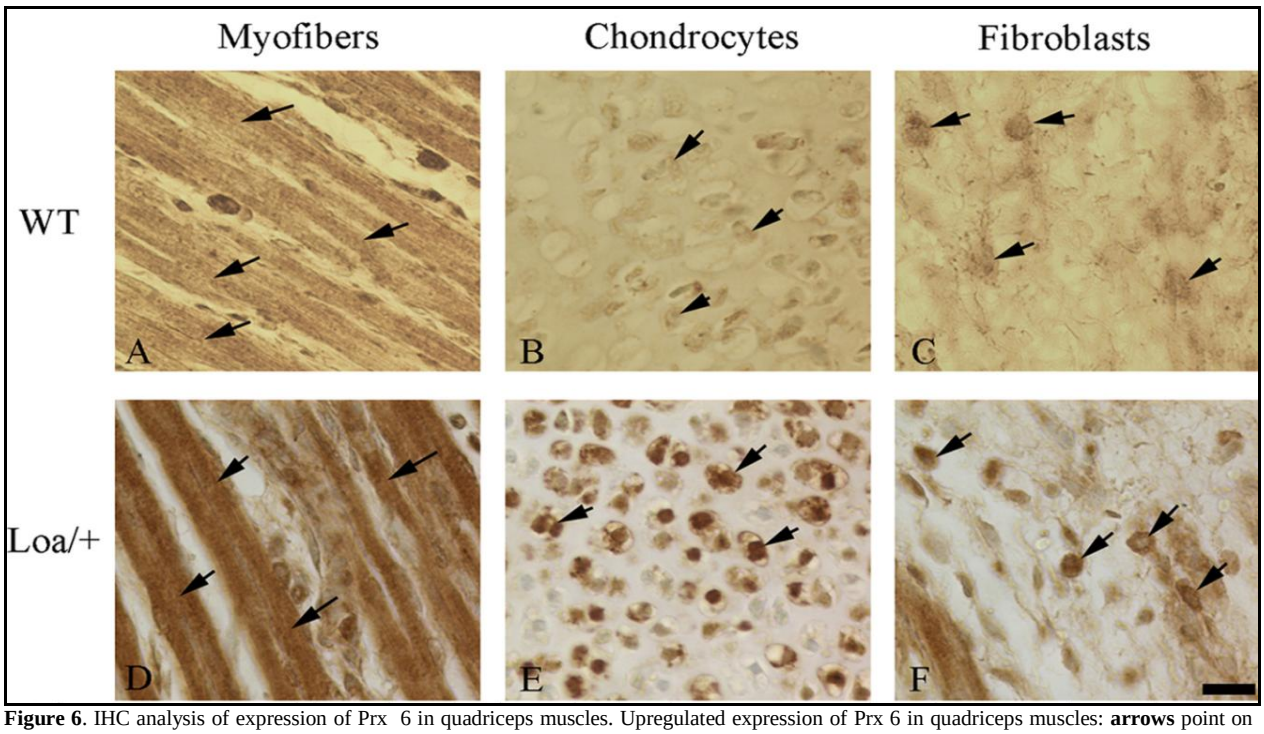


**Figure 6**. IHC analysis of expression of Prx 6 in quadriceps muscles. Upregulated expression of Prx 6 in quadriceps muscles: **arrows** point on myofibers **(AD)**, chondrocytes **(BE)**, and fibroblasts **(CF)**. (Scale bar 20 mm).

*Quadriceps muscle:* expression of Prx 6 in newborn Loa/+ mice was significantly increased in the sarcoplasm of myofibers (55.2 ± 4.04% *vs* 38.3 ± 3.23%, P = 0.008; Fig.5G, Figs.6AD), in the fibroblasts of perimysium (44.08 ± 2.21% *vs* 27.43 ± 3.64%. P = 0.001; Fig.5H, Figs.6CF), and in the chondrocytes of tendon (45.88 ± 4.56% *vs* 24.5 ± 2.01%, P = 0.002; Fig5D, Figs.6BE). Expression of Prx 6 was significantly decreased in the intercellular cartilage matrix (0.5 ± 0.1% *vs* 7 ± 1.16%, P = 0.004; Figs.6BE). Expression of Prx 6 was not significantly changed in the perimysium between fibroblasts (P = 0.314) and in satellite cells near myofibers (P = 0.529).

Taken together, these data indicate that motor neurons, dorsal root ganglion sensory neurons, glial cells surrounding them at the lumbar spinal cord level, and the quadriceps muscle of newborn Loa/+ mice experience oxidative stress, which may participate in morphological pathology and indicates an early onset of the disease.

## DISCUSSION

This study is the first to examine early pathological changes caused by the *DYNC1H* mutation on spinal lumbar motor neurons and sensory neurons of the dorsal root ganglion in newborn heterozygous Loa/+ mice at the ultrastructural level and to provide quantification of the expression of antioxidant proteins, such as Prxs 3, 5 and 6. We show that spinal lumbar sensory and motor neurons experience oxidative stress and display neuroinflammatory ultrastructural changes at an early postnatal stage. Here, we propose that chronic oxidative stress and inflammation may be involved in neurodegeneration of spinal lumbar neurons and lead to pathological changes in the quadriceps muscle and muscular tendon and this may contribute to the exacerbation of SMA-LED with age in human patients.

Accumulation of activated microglial cells around spinal motor neurons in ventral spinal cord indicates on acute neuroinflammation and acute stage of oxidative stress (Fig.7). Increased sizes of sensory neurons of the dorsal root ganglion indicate a mild neuroinflammation and mild oxidative stress (Fig.7). Other features of increased oxidative stress in motor and sensory neurons are an increased number of damaged mitochondria together with increased expression mitochondrial Prxs 3 and 5. Reduction of polyribosomes can lead to decrease of protein synthesis in spinal sensory and motor neurons in newborn Loa/+ mice. This reduction may be caused by alteration in attachment of ribosomes to cytoplasmic dynein and may also be the result of increased oxidative damage of motor proteins [36] and in this case is progressive with age, which is true for both human SMA-LED and mouse *DYNC1H*$^{Loa}$ mutations. Altered structure of endoplasmic reticulum is typical for a range of neurological disorders, including amyotrophic lateral sclerosis (ALS) [37, 38].

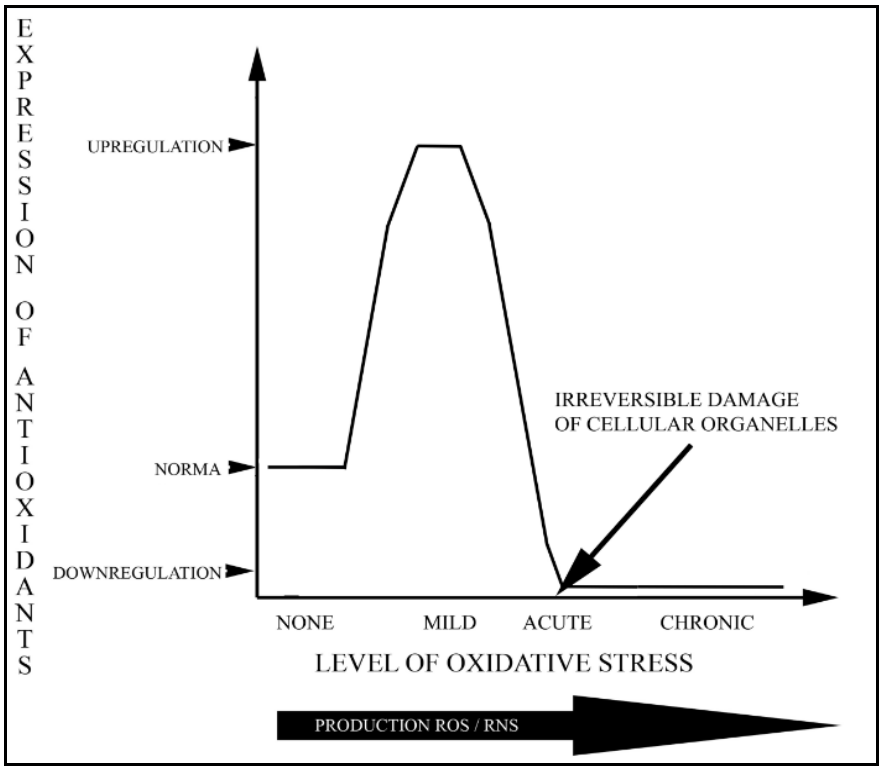


**Figure 7.**
Presumptive changes of expression of antioxidants in physiological and pathological conditions related to oxidative stress.
At normal physiological conditions an oxidative stress is absent.
Medium expression of antioxidants neutralize an oxidant's (*e.g.* ROS) production, as part of signaling pathways.
During early pathological stages (presymptomatic stage) an up-regulated expression of antioxidants tries to balance mild level of an oxidant's production.
During a symptomatic stage of pathologies related to oxidative stress natural antioxidant defense failed to protect tissues from oxidative damage and cause irreversible changes. This leads to chronic stage of pathologies (*e.g.* late stages of cystic fibrosis, cancer, aging) with depression of expression of antioxidants and elevated levels of oxidants.

 **DOI** 10.5455/oams.310714.or.071

Activated microglia cells are an additional source of ROS which produces oxidants through activation of NADPH-oxidase [39-41]. Microglia toxicity or microglia-mediated neuroinflammation are important components which increase oxidative stress and contribute to neurodegenerative and pathological conditions in the CNS [40-43]. Though activated microglia generate ROS and increase oxidative stress, it was shown that they also produce antioxidant proteins, such as Prxs 1, 2 and 5 to reduce oxidative stress [39, 44, 45]. This antagonistic feature of microglia was investigated in separate studies. In the text below and Fig.7 we discuss this opposite ability of glia to generate ROS and Prxs.

Immunohistochemical findings of this study indicate that not only astrocytes but also oligodendrocytes can express Prx 6 in lumbar spinal cord in both WT mice and Loa/+ mice. This finding in spinal cord confirms previously reported expression of Prx 6 in adult mouse brain [28]. Our data indicate that expression of Prx 6 in developmental spinal cord of newborn pups differ from the expression in adult spinal cord of mice [26, 32]. The dynein mutation of Loa/+ mice decreased the expression of Prx 6 in both macroglial cell types, especially in oligodendrocytes, located around motor neurons. The decreased expression of Prx 6 by macroglia may contribute to decreased levels of this protein in the extracellular space between the motor neurons and creation of toxic environment. Decreased expression of Prx 6 in oligodendrocytes, which form myelin sheath of axons in the CNS, may also contribute to change in its redox status and lead to oxidative damage of axons and neuromuscular junctions which are typical for Loa/+ mice.

Current findings show altered morphology and expression of the antioxidant proteins of the quadriceps muscle in early stage of the pathology. On the one hand, morphological changes of the quadriceps muscle point to muscle inflammation and early development of atrophy and denervation of the myofibers. On the other hand, increased expression Prx 6 indicates increased oxidative stress.

The expression of Prx 6 is altered under several pathological conditions [26, 30, 46-48]. In the neurodegeneration of ALS, the expression of Prx 6 was significantly up-regulated in astrocytes of the spinal cord in 6- to 8-week-old SOD1 transgenic mice [46]. The authors suggest that up-regulation of Prx 6 is a defensive antioxidant reaction. In addition, an *in vitro* study showed that astrocytes expressing mutated SOD1 kill spinal primary and embryonic mouse stem cell-derived motor neurons [49]. In this case it was proposed that astrocytes may play a role in the specific degeneration of spinal motor neurons in ALS, and identification of the astrocyte-derived soluble factor(s) may have far-reaching implications for ALS from both pathogenic and therapeutic standpoints [49]. We speculate that astrocytes of SOD1 transgenic mice produce a high amount of ROS which induce lipid peroxidation; this leads to chronic oxidative stress and causes death of motor neurons. The defensive antioxidant reaction, up-regulated expression of Prx 6, is not sufficient to prevent this process.

Previously, it was proposed that expression of Prx 6 increased in response to mild oxidative stress and decreased in response to severe oxidative stress [50]. A similar mechanism was proposed for other antioxidant proteins in pathological conditions [51-53]. Our data indicate that the lumbar spinal sensory neurons, the quadriceps muscle and the muscular tendon encounter mild oxidative stress at this early stage of the pathology, while the motor neurons of the ventral horn are exposed to acute oxidative stress in the lumbar spinal cord. Similar to astrocytes of SOD1 transgenic mice, macro- and microglia of Loa/+ mice first generate ROS and reactive nitrogen species (RNS) and increase oxidative stress, and later they express antioxidant proteins, including Prxs, to repair damage caused by oxidants (Fig.7).

Although Loa/+ mice and SOD1 transgenic mice are mouse models for different diseases, our data indicate that these mutations have some similar pathological features, such as altered expression of secretory Prx 6 by macroglial cells located around degenerating motor neurons which point to increased oxidative stress. Ability of glia to express other types of Prxs, such as Prx 1, 2, 4 and 5, was shown in other pathologies [39, 44, 45, 54-56]. These changes in expression of Prxs point to its diversity and distinct functional roles in different pathologies, including neurological and neurodegenerative diseases [30].

Fig.7 presents a model of oxidative stress, which explains altered expression of Prxs in relationship with level of oxidative stress in our study. Under physiological conditions, an intermediate level of antioxidants and oxidants is generated; both of them are important for cellular signaling. Under pathological conditions (for example early stages of SMA-LED during embryogenesis and early childhood) there is an increase in the generation of oxidants followed by an increased expression of antioxidants. This condition is the first stage of oxidative stress (mild oxidative stress) and this condition is reversible if sufficient amounts of the antioxidant proteins are present. If not, it leads to development of acute oxidative stress with a significant imbalance: increased amount of oxidants and decreased amount of antioxidants and in this stage of oxidative stress there typically is irreversible damage of cellular organelles. When these conditions exist for a longer time, the severe imbalance persists and causes chronic oxidative stress, which leads to cell death.

**How do the data of our current research fit with the pathological mechanism of Loa/+ mutation?**

Fig.8 shows the pathological mechanism of Loa/+ mutation and interaction between motor neurons and glia. Motor neurons of Loa/+ mice are more susceptible to oxidative stress caused by the dynein mutation because it slows down the retrograde traffic of mitochondria to cell body for recycling and thereby causes damage of mitochondria and increased "leakage" of superoxide anion and ROS into the cytoplasm [57]. Then, in the cytoplasm superoxide anions and ROS start free radical chain reactions, which damage cellular organelles, RNA, DNA, proteins, lipids and membranes.

Comparison of the two mutant mice, namely $SOD1^{G93A}$ and $DYNC1H^{Loa}$ + $SOD1^{G93A}$ (double mutation), point to the importance of retrograde transport of mitochondria. $SOD1^{G93A}$ mice have mitochondrial *SOD1* mutation, axonal transport defects and short lifespan [6, 58]. Mice with $DYNC1H^{Loa}$ and $SOD1^{G93A}$ double mutation have restoration of the retrograde transport of cellular organelles, including mitochondria, to neuronal cell body where autophagic recycling of mitochondria occurs [59] and consequently leads to significant reduction of SOD1 protein which is located in the mitochondrial matrix [9] that determine amelioration of pathology of deadly $SOD1^{G93A}$ mutation with significant increase in life extension [6].

A high level of energy metabolism, increased number of mitochondria, lack of catalase (CAT), lower rates of regeneration [57] and large size of motor neurons aggravate oxidative stress in the motor neurons. During normal aging, human tissues show a decrease in expression and activity (due to overoxidation) of antioxidant proteins, particularly Prxs, but not SOD and CAT [60-63], and increase generation of ROS [64-66]; neurons became less protective from oxidative stress which leads to typical increase of neurodegenerative diseases with age.

A recent study shows that a natural activator of the antioxidant enzyme Prx 6 is glutathione S-transferase (GST) pi [25]. At a pre-symptomatic age (70 days), expression of this protein was unchanged, but it was decreased at a symptomatic age (140 days) in SOD1 mice, but not in Cra1/SOD1 mice. Expression of this protein was stable in the spinal cord of Cra1 mutant mice when compared with WT mice [67]; the authors conclude that the *DYNC1H1* mutation reduces the toxic effects caused by the SOD1 mutation in Cra1/SOD1 mice. Because of the similarity of Loa and Cra1 mutations, it is possible that Loa/+ mice also have a normal level of expression of GST pi. A deficit in Prx 6, but not of its activator may regulate neurodegeneration in Loa/+ mice.

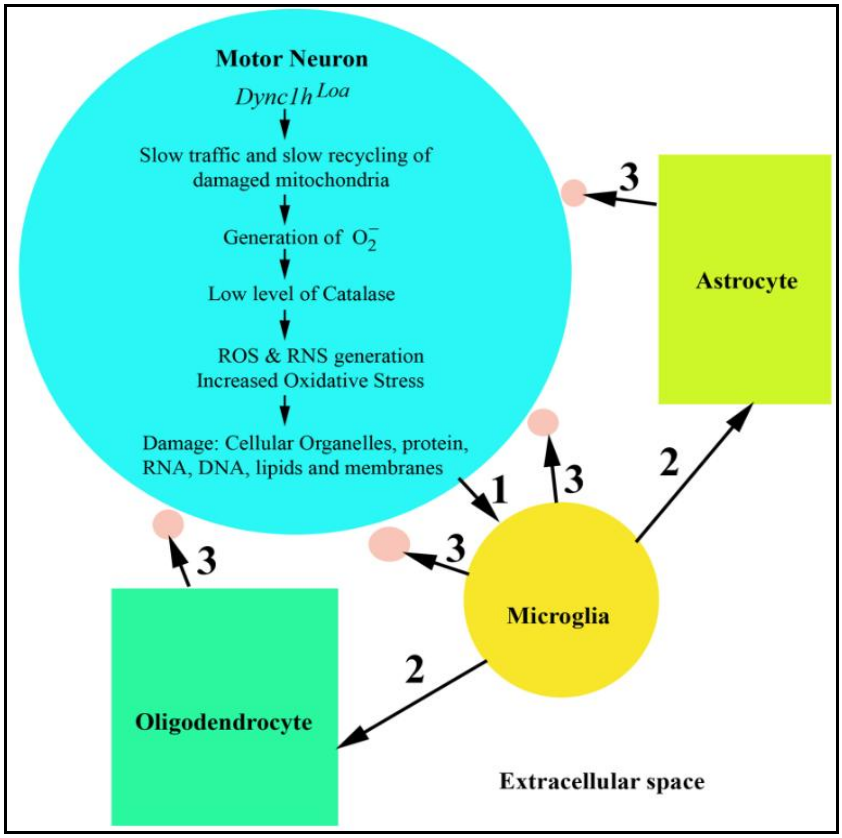


**Figure 8.**
Presumptive pathological mechanism of the Loa/+ mutation.
**(1)** Damaged or modified proteins activate microglia in a receptor-mediated way.
**(2)** Activated microglia send signals that activate astrocytes and oligodendrocytes.
**(3)** Increased generation of ROS and secretion into extracellular space between neurons cause neuroinflammation.

 **DOI** 10.5455/oams.310714.or.071

The data presented in the current study suggest that decrease in secretion of Prx 6 by macroglia leads to a decrease in the amount of this protein in the extracellular space surrounding motor neurons at early stages of the pathology and leads to development of toxic conditions such as chronic oxidative stress, and this may cause degeneration of lumbar motor neurons. Thus, a deficit of Prx 6 may be detrimental to the survival of motor neurons and cause progression of the pathology, and may be a key target for future therapeutic strategies to address symptoms of the *DYNC1H1* mutation [68]. A similar mechanism was proposed for degeneration of motor neurons in ALS [69].

Pathological findings from muscles of human patients with the SMA-LED also indicate a possible deficit of Prx 6, where a massive increase in the amount of fibrous tissue, lipid degeneration and replacement of muscle by fat tissue was described [1, 3-5]. Since Prx 6 can prevent accumulation of fibroblasts in fibrous tissue [70], and can decrease lipid degeneration by turnover of lipid peroxidation [25], we propose that exogenous administration of Prx 6 at early stages of SMA-LED may reduce pathology in the muscle and decrease degeneration of motor neurons. Because it was suggested that early diagnosis and proactive care extend significantly the lifespan of SMA patients, and treatment at the neonatal stage is an option [71], we predict that preventive therapeutic interventions in fetuses, infants and children may be the most effective.

The data on newborn Loa/+ mice suggest a protective function of Prx 6 in motor neuron disease models. The significant decrease in glial and extracellular Prx 6 expression in early stages of the pathology is consistent with the hypothesis that chronic oxidative stress may lead to neurodegeneration of motor neurons. Accordingly, we predict that exogenous administration of this protein will ameliorate oxidative stress and pathology in an animal model of SMA-LED and may be considered as new approach in future pediatric therapeutic interventions to prevent progression of the disease.

**ACKNOWLEDGEMENTS**

Dr. Majid Hafezparast from School of Life Sciences, University of Sussex UK, for generously providing mice for experiments and discussion of the results, Drs. Christopher Von Bartheld and Elisabeth Fisher for support of the project and Dr. Thomas Gould for advice on dissection of sensory ganglia and critical reading of the manuscript.

The project was supported by a junior faculty research grant from the University of Nevada, School of Medicine and NIH grants GM103554 and GM103440.

**CONFLICTS OF INTEREST**

The author declares that she have no conflict of interest.

**REFERENCES**

1. Harms MB, Ori-McKenney KM, Scoto M, Tuck EP, Bell S, Ma D, Masi S, Allred P, Al-Lozi M, Reilly MM, Miller LJ, Jani-Acsadi A, Pestronk A, Shy ME, Muntoni F, Vallee RB, Baloh RH. Mutations in the tail domain of DYNC1H1 cause dominant spinal muscular atrophy. Neurology 2012; 78:1714-20.
2. Hoffman EP, Talbot K. A calm before the exome storm: coming together of dSMA and CMT2. Neurology 2012; 78:1706-7.
3. Tsurusaki Y, Saitoh S, Tomizawa K, Sudo A, Asahina N, Shiraishi H, Ito J, Tanaka H, Doi H, Saitsu H, Miyake N, Matsumoto N. A *DYNC1H1* mutation causes a dominant spinal muscular atrophy with lower extremity predominance. Neurogenetics 2012; 13:327-32.
4. Harms MB, Allred P, Gardner R Jr, Fernandes Filho JA, Florence J, Pestronk A, Al-Lozi M, Baloh RH. Dominant spinal muscular atrophy with lower extremity predominance: linkage to 14q32. Neurology 2010; 75:539-46.
5. Fiorillo C, Moro F, Yi J, Weil S, Brisca G, Astrea G, Severino M, Romano A, Battini R, Rossi A, Minetti C, Bruno C, Santorelli FM, Vallee R. Novel dynein DYNC1H1 neck and motor domain mutations link distal spinal muscular atrophy and abnormal cortical development. Hum Mutat 2014; 35:298-302.
6. Schiavo G, Greensmith L, Hafezparast M, Fisher EM. Cytoplasmic dynein heavy chain: the servant of many masters. Trends Neurosci 2013; 36:641-51.
7. Rogers DC, Peters J, Martin JE, Ball S, Nicholson SJ, Witherden AS, Hafezparast M, Latcham J, Robinson TL, Quilter CA, Fisher EM. SHIRPA, a protocol for behavioral assessment: validation for longitudinal study of neurological dysfunction in mice. Neurosci Lett 2001; 306:89-92.
8. Hafezparast M, Klocke R, Ruhrberg C, Marquardt A, Ahmad-Annuar A, Bowen S, Lalli G, Witherden AS, Hummerich H, Nicholson S, Morgan PJ, Oozageer R, Priestley JV, Averill S, King VR, Ball S, Peters J, Toda T, Yamamoto A, Hiraoka Y, Augustin M, Korthaus D, Wattler S, Wabnitz P, Dickneite C, Lampel S, Boehme F, Peraus G, Popp A, Rudelius M, Schlegel J, Fuchs H, Hrabe de Angelis M, Schiavo G, Shima DT, Russ AP, Stumm G, Martin JE, Fisher EM. Mutations in dynein link motor neuron degeneration to defects in retrograde transport. Science 2003; 300:808-12.
9. El-Kadi AM, Bros-Facer V, Deng W, Philpott A, Stoddart E, Banks G, Jackson GS, Fisher EM, Duchen MR, Greensmith L, Moore AL, Hafezparast M. The legs at odd angles (Loa) mutation in cytoplasmic dynein ameliorates mitochondrial function in SOD1G93A mouse model for motor neuron disease. J Biol Chem 2010; 285:18627-39.
10. Eschbach J, Fergani A, Oudart H, Robin JP, Rene F, Gonzalez de Aguilar JL, Larmet Y, Zoll J, Hafezparast M, Schwalenstocker B, Loeffler JP, Ludolph AC, Dupuis L. Mutations in cytoplasmic dynein lead to a Huntington's disease-like defect inenergy metabolism of brown and white adipose tissues. Biochim Biophys Acta 2011; 1812:59-69.
11. Chen XJ, Levedakou EN, Millen KJ, Wollmann RL, Soliven B, Popko B. Proprioceptive sensory neuropathy in mice with a mutation in the cytoplasmic Dynein heavy chain 1 gene. J Neurosci 2007; 27:14515-24.
12. Courchesne SL, Pazyra-Murphy MF, Lee DJ, Segal RA. Neuromuscular junction defects in mice with mutation of dynein heavy chain 1. PLoS One 2011; 6:e16753.
13. Wiggins LM, Kuta A, Stevens JC, Fisher EM, von Bartheld CS. A novel phenotype for the dynein heavy chain mutation Loa: altered dendritic morphology, organelle density, and reduced numbers of trigeminal motoneurons. J Comp Neurol 2012; 520:2757-73.

**14.** Wong PC, Pardo CA, Borchelt DR, Lee MK, Copeland NG, Jenkins NA, Sisodia SS, Cleveland DW, Price DL. An adverse property of a familial ALS-linked SOD1 mutation causes motor neuron disease characterized by vacuolar degeneration of mitochondria. Neuron 1995; 14:1105-16.

**15.** Kong J, Xu Z. Massive mitochondrial degeneration in motor neurons triggers the onset of amyotrophic lateral sclerosis in mice expressing a mutant SOD1. J Neurosci 1998; 18:3241-50.

**16.** Barber SC, Mead RJ, Shaw PJ. Oxidative stress in ALS: a mechanism of neurodegeneration and a therapeutic target. Biochim Biophys Acta 2006; 1762:1051-67.

**17.** Teuchert M, Fischer D, Schwalenstoecker B, Habisch HJ, Böckers TM, Ludolph AC. A dynein mutation attenuates motor neuron degeneration in SOD1(G93A) mice. Exp Neurol 2006; 198:271-4.

**18.** Terry AV Jr. Neurodegeneration. Encyclopedia of Molecular Pharmacology. Springer, Berlin-Heidelberg-New York, pp 822-827, 2008.

**19.** Federico A, Cardaioli E, Da Pozzo P, Formichi P, Gallus GN, Radi E. Mitochondria, oxidative stress and neurodegeneration. J Neurol Sci 2012; 322:254-62.

**20.** Eschbach J, Sinniger J, Bouitbir J, Fergani A, Schlagowski AI, Zoll J, Geny B, Rene F, Larmet Y, Marion V, Baloh RH, Harms MB, Shy ME, Messadeq N, Weydt P, Loeffler JP, Ludolph AC, Dupuis L. Dynein mutations associated with hereditary motor neuropathies impair mitochondrial morphology and function with age. Neurobiol Dis 2013; 58:220-30.

**21.** Drechsel DA, Patel M. Respiration-dependent $H_2O_2$ removal in brain mitochondria via the thioredoxin/peroxiredoxin system. J Biol Chem 2010; 285:27850-8.

**22.** Angeles DC, Gan BH, Onstead L, Zhao Y, Lim KL, Dachsel J, Melrose H, Farrer M, Wszolek ZK, Dickson DW, Tan EK. Mutations in LRRK2 increase phosphorylation of peroxiredoxin 3 exacerbating oxidative stress-induced neuronal death. Hum Mutat 2011; 32:1390-7.

**23.** Lopert P, Day BJ, Patel M. Thioredoxin reductase deficiency potentiates oxidative stress, mitochondrial dysfunction and cell death in dopaminergic cells. PLoS One 2012; 7:e50683.

**24.** Liu G, Feinstein SI, Wang Y, Dodia C, Fisher D, Yu K, Ho YS, Fisher AB. Comparison of glutathione peroxidase 1 and peroxiredoxin 6 in protection against oxidative stress in the mouse lung. Free Radic Biol Med 2010; 49:1172-81.

**25.** Fisher AB. Peroxiredoxin 6: a bifunctional enzyme with glutathione peroxidase and phospholipase $A_2$ activities. Antioxid Redox Signal 2011; 15:831-44.

**26.** Yata K, Oikawa S, Sasaki R, Shindo A, Yang R, Murata M, Kanamaru K, Tomimoto H. Astrocytic neuroprotection through induction of cytoprotective molecules; a proteomic analysis of mutant P301S tau-transgenic mouse. Brain Res 2011; 1410:12-23.

**27.** Elkharaz J, Ugun-Klusek A, Constantin-Teodosiu D, Lawler K, Mayer RJ, Billett E, Lowe J, Bedford L. Implications for oxidative stress and astrocytes following 26S proteasomal depletion in mouse forebrain neurones. Biochim Biophys Acta 2013; 1832:1930-8.

**28.** Jin MH, Lee YH, Kim JM, Sun HN, Moon EY, Shong MH, Kim SU, Lee SH, Lee TH, Yu DY, Lee DS. Characterization of neural cell types expressing peroxiredoxins in mouse brain. Neurosci Lett 2005; 381:252-7.

**29.** Power JH, Asad S, Chataway TK, Chegini F, Manavis J, Temlett JA, Jensen PH, Blumbergs PC, Gai WP. Peroxiredoxin 6 in human brain: molecular forms, cellular distribution and association with Alzheimer's disease pathology. Acta Neuropathol 2008; 115:611-22.

**30.** Krapfenbauer K, Engidawork E, Cairns N, Fountoulakis M, Lubec G. Aberrant expression of peroxiredoxin subtypes in neurodegenerative disorders. Brain Res 2003; 967:152-60.

**31.** Hwang IK, Yoo KY, Kim DW, Lee CH, Choi JH, Kwon YG, Kim YM, Choi SY, Won MH. Changes in the expression of mitochondrial peroxiredoxin and thioredoxin in neurons and glia and their protective effects in experimental cerebral ischemic damage. Free Radic Biol Med 2010; 48:1242-51.

**32.** Fang KM, Chen JK, Hung SC, Chen MC, Wu YT, Wu TJ, Lin HI, Chen CH, Cheng H, Yang CS, Tzeng SF. Effects of combinatorial treatment with pituitary adenylate cyclase activating peptide and human mesenchymal stem cells on spinal cord tissue repair. PLoS One 2010; 5:e15299.

**33.** Nguyen DH, Zhou T, Shu J, Mao JH. Quantifying chromogen intensity in immunohistochemistry via reciprocal intensity. Cancer InCytes 2013; 2(1):e.

**34.** Matkowskyj KA, Schonfeld D, Benya RV. Quantitative immunohistochemistry by measuring cumulative signal strength using commercially available software photoshop and matlab. J Histochem Cytochem 2000; 48:303-12.

**35.** DeGirolami UU, Smith TW. Teaching monograph: pathology of skeletal muscle diseases. Am J Pathol 1982; 107:231-76.

**36.** Hauss-Wegrzyniak B, Vannucchi MG, Wenk GL. Behavioral and ultrastructural changes induced by chronic neuroinflammation in young rats. Brain Res 2000; 859:157-66.

**37.** Roussel BD, Kruppa AJ, Miranda E, Crowther DC, Lomas DA, Marciniak SJ. Endoplasmic reticulum dysfunction in neurological disease. Lancet Neurol 2013; 12:105-18.

**38.** Dodson M, Darley-Usmar V, Zhang J. Cellular metabolic and autophagic pathways: traffic control by redox signaling. Free Radic Biol Med 2013; 63:207-21.

**39.** Ock J, Han HS, Hong SH, Lee SY, Han YM, Kwon BM, Suk K. Obovatol attenuates microglia-mediated neuroinflammation by modulating redox regulation. Br J Pharmacol 2010; 159:1646-62.

**40.** Peterson LJ, Flood PM. Oxidative stress and microglial cells in Parkinson's disease. Mediators Inflamm 2012; 2012:401264.

**41.** Qin L, Liu Y, Hong JS, Crews FT. NADPH oxidase and aging drive microglial activation, oxidative stress, and dopaminergic neurodegeneration following systemic LPS administration. Glia 2013; 61:855-68.

**42.** Stoll G, Jander S. The role of microglia and macrophages in the pathophysiology of the CNS. Prog Neurobiol 1999; 58:233-47.

**43.** Zheng LT, Ock J, Kwon BM, Suk K. Suppressive effects of flavonoid fisetin on lipopolysaccharide-induced microglial activation and neurotoxicity. Int Immunopharmacol 2008; 8:484-94.

**44.** Kim SU, Hwang CN, Sun HN, Jin MH, Han YH, Lee H, Kim JM, Kim SK, Yu DY, Lee DS, Lee SH. Peroxiredoxin I is an indicator of microglia activation and protects against hydrogen peroxide-mediated microglial death. Biol Pharm Bull 2008; 31:820-5.

**45.** Sun HN, Kim SU, Huang SM, Kim JM, Park YH, Kim SH, Yang HY, Chung KJ, Lee TH, Choi HS, Min JS, Park MK, Kim SK, Lee SR, Chang KT, Lee SH, Yu DY, Lee DS. Microglial peroxiredoxin V acts as an inducible anti-inflammatory antioxidant through cooperation with redox signaling cascades. J Neurochem 2010; 114:39-50.

**46.** Strey CW, Spellman D, Stieber A, Gonatas JO, Wang X, Lambris JD, Gonatas NK. Dysregulation of stathmin, a microtubule-destabilizing protein, and up-regulation of Hsp25, Hsp27, and the antioxidant peroxiredoxin 6 in a mouse model of familial amyotrophic lateral sclerosis. Am J Pathol 2004; 165:1701-18.


 **DOI** 10.5455/oams.310714.or.071

**47.** Yoon S, Cong WT, Bang Y, Lee SN, Yoon CS, Kwack SJ, Kang TS, Lee KY, Choi JK, Choi HJ. Proteome response to ochratoxin A-induced apoptotic cell death in mouse hippocampal HT22 cells. Neurotoxicology 2009; 30:666-76.

**48.** Pal A, Fontanilla D, Gopalakrishnan A, Chae YK, Markley JL, Ruoho AE. The sigma-1 receptor protects against cellular oxidative stress and activates antioxidant response elements. Eur J Pharmacol 2012; 682:12-20.

**49.** Nagai M, Re DB, Nagata T, Chalazonitis A, Jessell TM, Wichterle H, Przedborski S. Astrocytes expressing ALS-linked mutated SOD1 release factors selectively toxic to motor neurons. Nat Neurosci 2007; 10:615-22.

**50.** Trudel S, Kelly M, Fritsch J, Nguyen-Khoa T, Thérond P, Couturier M, Dadlez M, Debski J, Touqui L, Vallée B, Ollero M, Edelman A, Brouillard F. Peroxiredoxin 6 fails to limit phospholipid peroxidation in lung from Cftr-knockout mice subjected to oxidative challenge. PLoS One 2009; 4:e6075.

**51.** Chaiswing L, Zhong W, Oberley TD. Increasing discordant antioxidant protein levels and enzymatic activities contribute to increasing redox imbalance observed during human prostate cancer progression. Free Radic Biol Med 2013; 67:342-52.

**52.** Liu JQ, Zheng SQ, Sang YZ, Sun Y, Zhang HW, Xiong YJ, Yi Y, Wang JR. Expression of peroxiredoxin I in the rats exposed to silica. Zhonghua Lao Dong Wei Sheng Zhi Ye Bing Za Zhi 2013; 31:531-3.

**53.** Wojcik KA, Kaminska A, Blasiak J, Szaflik J, Szaflik JP. Oxidative stress in the pathogenesis of keratoconus and Fuchs endothelial corneal dystrophy. Int J Mol Sci 2013; 14:19294-308.

**54.** Rohl C, Armbrust E, Kolbe K, Lucius R, Maser E, Venz S, Gulden M. Activated microglia modulate astroglial enzymes involved in oxidative and inflammatory stress and increase the resistance of astrocytes to oxidative stress *in vitro*. Glia 2008; 56:1114-26.

**55.** Holley JE, Newcombe J, Winyard PG, Gutowski NJ. Peroxiredoxin V in multiple sclerosis lesions: predominant expression by astrocytes. Mult Scler 2007; 13:955-61.

**56.** Rowe DD, Leonardo CC, Hall AA, Shahaduzzaman MD, Collier LA, Willing AE, Pennypacker KR. Cord blood administration induces oligodendrocyte survival through alterations in gene expression. Brain Res 2010; 1366:172-88.

**57.** Milani P, Ambrosi G, Gammoh O, Blandini F, Cereda C. SOD1 and DJ-1 converge at Nrf2 pathway: a clue for antioxidant therapeutic potential in neurodegeneration. Oxid Med Cell Longev 2013; 2013:836760.

**58.** Kieran D, Hafezparast M, Bohnert S, Dick JR, Martin J, Schiavo G, Fisher EM, Greensmith L. A mutation in dynein rescues axonal transport defects and extends the life span of ALS mice. J Cell Biol 2005; 169:561-7.

**59.** Terman A, Dalen H, Eaton JW, Neuzil J, Brunk UT. Mitochondrial recycling and aging of cardiac myocytes: the role of autophagocytosis. Exp Gerontol 2003; 38:863-76.

**60.** Lu JL, Vallat JM, Pollard JD, Knoops B, Ouvrier R. Expression of the antioxidant enzyme peroxiredoxin 5 in the human peripheral nervous system. J Peripher Nerv Syst 2006; 11:318-24.

**61.** Yoo KY, Park OK, Yu J, Yan B, Li H, Lee CH, Choi JH, Kim DW, Hwang IK, Won MH. Expression and changes of hyperoxidized peroxiredoxins in non-pyramidal and polymorphic cells in the gerbil hippocampus during normal aging. Cell Mol Neurobiol 2009; 29:413-21.

**62.** Lim J, Luderer U. Oxidative damage increases and antioxidant gene expression decreases with aging in the mouse ovary. Biol Reprod 2011; 84:775-82.

**63.** Nystrom T, Yang J, Molin M. Peroxiredoxins, gerontogenes linking aging to genome instability and cancer. Genes Dev 2012; 26:2001-8.

**64.** Knight JA. The biochemistry of aging. Adv Clin Chem 2000; 35:1-62.

**65.** Andersen JK. Oxidative stress in neurodegeneration: cause or consequence? Nat Med 2004; 10:S18-25.

**66.** Poon HF, Calabrese V, Scapagnini G, Butterfield DA. Free radicals: key to brain aging and heme oxygenase as a cellular response to oxidative stress. J Gerontol A Biol Sci Med Sci 2004; 59:478-93.

**67.** Kazmierczak B, Kuzma-Kozakiewicz M, Usarek E, Baranczyk-Kuzma A. Differences in glutathione S-transferase pi expression in transgenic mice with symptoms of neurodegeneration. Acta Biochim Pol 2011; 58:621-6.

**68.** Fiorillo C, Moro F, Yi J, Weil S, Brisca G, Astrea G, Severino M, Romano A, Battini R, Rossi A, Minetti C, Bruno C, Santorelli FM, Vallee R. Novel dynein DYNC1H1 neck and motor domain mutations link distal spinal muscular atrophy and abnormal cortical development. Hum Mutat 2014; 35:298-302.

**69.** Miquel E, Cassina A, Martinez-Palma L, Bolatto C, Trías E, Gandelman M, Radi R, Barbeito L, Cassina P. Modulation of astrocytic mitochondrial function by dichloroacetate improves survival and motor performance in inherited amyotrophic lateral sclerosis. PLoS One 2012; 7:e34776.

**70.** Novoselov VI, Baryshnikova LM, Yanin VA, Amelina SE, Fesenko EE. The influence of peroxyredoxin VI on incised-wound healing in rats. Dokl Biochem Biophys 2003; 393:326-7.

**71.** Kayadjanian N, Burghes A, Finkel RS, Mercuri E, Rouault F, Schwersenz I, Talbot K. SMA-EUROPE workshop report: Opportunities and challenges in developing clinical trials for spinal muscular atrophy in Europe. Orphanet J Rare Dis 2013; 8:44.